Numerical Analysis of Pulsatile Blood Flow in a Stented Human Coronary Artery with a Flow Divider

Vahab Dehlaghi, Mohammad Tafazoli Shadpoor and Siamak Najarian
Department of Biomechanics, Faculty of Biomedical Engineering
Amirkabir University of Technology, Tehran, Iran

Abstract: Shear stress is known to play a central role in restenosis formation and is sensitive to stent geometry. Local flow alterations created by a different stents without and with flow divider were studied to compare the hemodynamic effects of Stent design properties on restenosis in stented human coronary artery. Blood pressure and shear stress values were computed in three different sites, including stented arterial segment, pre-stent and post-stent regions using computational fluid dynamics. Blood flow was assumed as pulsatile, incompressible and Newtonian flow. Rigid boundary conditions were assumed for all models. The governing Navier-Stokes equations were solved using commercial software package (Fluent V6.0.12). Stents are assumed with real structure and modeled using the commercial software package (Gambit, V2.0). The arterial wall shear stress distribution was investigated in three major regions and critical sites were located. It is concluded that the wall shear stress between stent struts was sensitive to strut spacing, profile of strut, number of struts and curvature. Our 3D computational fluid dynamics modeling demonstrate that with increasing the angle between two sides of the stent strut the percentage of intrastrut area that exposed to critical value of *WSS* decreases. By application of a flow divider, the wall shear stress in stented segment increases markedly and so is the pressure gradient in stented segment. Flow divider influences the blood flow pattern in proximal of stented segment. In this section, the *WSS* increases with application of the flow divider. The results for different diameters of flow divider show that optimum diameter for flow divider is *D/3*.

Key words: Stent, shear stress, restenosis, coronary artery, computational fluid dynamics.

INTRODUCTION

Atherosclerosis is a vascular disease that reduces arterial lumen size through plaque formation and arterial wall thickening. The pathological complications of atherosclerosis, namely heart disease and stroke, remain the leading cause of mortality in the western world. Various studies have shown that independently of systemic factors, the presence of local hemodynamic factors such as wall shear stress plays a major role in the generation, progression and destabilization of atherosclerotic plaques[1, 2, 3]. Areas with low wall shear stress (<1.26 Pa) displayed a significant increase in the thickness of the atherosclerotic plaque and the vessel wall (positive remodeling). Areas with physiologic wall shear stress (1.26-2.69 Pa) did not display significant changes and areas exposed to a high wall shear stress ($\geq$ 2.7 Pa) displayed positive remodeling of the artery without changes in the atheroma plaque[4].

A common interventional procedure against advanced atherosclerosis involves the placement of an intravascular stent. Intravascular stents, which are small tube-like structures, can be placed into stenotic arteries to restore blood flow perfusion to the downstream tissues. The reasons for the routine clinical implementation of coronary stents include:

1. Stents provide favorable and predictable acute angiographic results.
2. Stents improve the safety of angioplasty by successfully treating acute and threatened closure.
3. Stents improve long-term clinical outcomes by reducing restenosis.
4. Stents are easy to use.
5. The use of stents often decreases total procedure time.
6. Stents provide favorable angiographic and clinical results in most complex lesion morphologies that are poorly treated using conventional balloon

Corresponding Author: Siamak Najarian, Full-Professor of Biomedical Engineering, No. 424, Hafez Avenue, Department of Biomechanics, Faculty of Biomedical Engineering, Amirkabir University of Technology, Tehran, Iran, P.O. Box 15875-4413

angioplasty techniques (i.e., saphenous vein graft lesions, ostial stenosis, eccentric lesions and total occlusions).

The increase in the popularity of coronary stenting as a primary treatment modality and the application of stenting techniques to a broader and more complex range of lesion types have prompted industry to respond with a plethora of innovative and competitive stent designs. Presently, there are more than 55 standard and customized stent types, manufactured by 28 different companies, available for use in the coronary system. Most of these devices are second or third generation, with designs that are undergoing evolution as stent technology advances.

Restenosis following implantation of coronary stents is mainly due to a process of neointimal proliferation within and at the edges of the stent. The variables that have been associated with this process include systemic factors, such as hypertension, diabetes, blood pressure, aging, increased levels of plasma cholesterol and hemodynamics[5-8]. Both *in vitro* and *in vivo* studies have revealed that stent structure influences global and local flow patterns, thrombus accumulation between struts and restenosis[9,10]. Recently, coronary restenosis in patients receiving a variety of stent types was shown to be most dependent on vessel size and stent design[11-15]. Artery wall shear stress concentrations can provoke tissue response that may lead to stent restenosis. It is also clear that local blood flow patterns are affected by stent design; hence, the relationships between blood flow patterns, stent design and the process of restenosis should be investigated thoroughly. Although it is difficult to verify conclusively such relationships without suitable *in vivo* studies, CFD can provide an excellent research tool to help understand these underlying issues. The *in vivo* studies have confirmed that an increase of the local shear stress reduces the neointimal formation[16-18].

CFD is being employed by several researchers to explore further the nature of flow stagnation patterns on stent strut shape and spacing[19-22]. These studies have confirmed that the flow stagnation patterns between stent struts depend most strongly on stent strut spacing and have demonstrated that vessel wall compliance has little effect on these flow patterns. Most previous stent CFD research studies have not included the complex real geometries that are present during actual clinical interventional procedures. Instead, most studies consider simplified and idealized geometry. Although this can provide a great deal of information, fully three-dimensional studies need to be considered.

This investigation presents comprehensive 3D computational fluid dynamics models to analyze blood flow and *WSS* values in models of stented human coronary artery with differing geometrical parameters and flow divider.

MATERIALS AND METHODS

CFD modeling was applied to investigate the steady flow field in the vicinity of stents placed within arterial segments in a coronary artery model. In 2D simulations, stents were modeled as series of rigid rings with different shapes and stent strut spacings located within straight and curved rigid-walled models of arterial segments. In all models, H denotes the stent wire thickness, W indicates the stent inter-ring width and D denotes the arterial diameter (Fig. 1). The model includes a vessel length of $2D$ both upstream and downstream of the stented segment. The curvature angle is:

$$\theta = \frac{L}{R} \qquad (1)$$

where,
L: artery length (constant)
R: Curvature radius
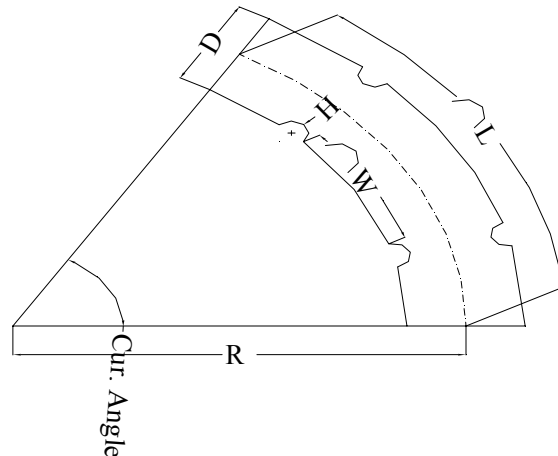Θ: curvature angel (30˚, 60˚, 90˚)

Fig. 1: The 2D stents geometry

The 3D dimensional view of stents with a flow divider is shown in Fig. 2. In 3D simulations, stents were modeled with real structure. We used the GAMBIT (version 2.0) software to make these models. We defined the special points on stent area and by connecting these points to each other and defining the necessary wires, the real profile for a stent strut was
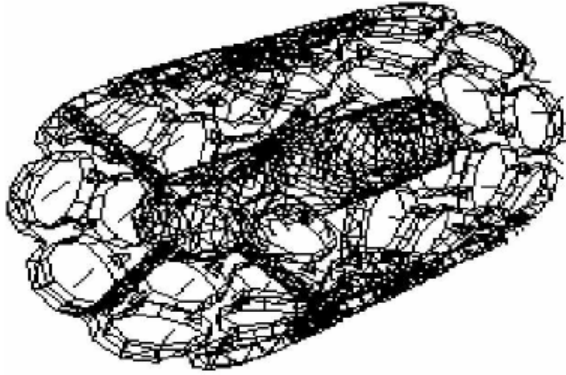
Fig. 2: Model of stent with flow divider

plotted. Transferring and rotating of loops prepared the requested diameter and length of stents. The default stent was transferred to a vessel with the same diameter. The combination of this vessel and stent is like a vessel that a stent was implanted on it. The flow divider (Anti-Restenotic Diffuser, EndoArt, Lausanne, Switzerland) is a flexible cylindrical body with different diameters and lengths, which is centered within the stent lumen by means of self-expandable stabilizing arms (Fig. 2). The flow domains for the normal and stented vessels were discretized with T-grid algorithm of commercial software GAMBIT. GAMBIT allows us to specify any volume for a meshing operation; however, the shape and topological characteristics of the volume, as well as the vertex types associated with its faces, determine the type(s) of mesh scheme(s) that can be applied to the volume. To specify the meshing scheme, one must specify two parameters elements and type. The elements parameter defines the shape(s) of the elements that are used to mesh the volume. The type parameter defines the meshing algorithm and therefore, the overall pattern of mesh elements in the volume. When one specifies a volume on the Mesh Volumes form, GAMBIT automatically evaluates the volume with respect to its shape, topological characteristics and vertex types and sets the scheme option buttons to reflect a recommended volume meshing scheme. By attention to stented artery geometry, GAMBIT automatically allows us to specify the Tet/Hybrid volume meshing elements options and T-Grid volume meshing type options. Grid sensitivity tests showed a variation of less than 1% in the solution of the parameters of interest when the size of volumes decreased 10% (495,846 mesh volume increased to 545,430 mesh volume). The blood flow was modeled as an incompressible Newtonian viscous fluid governed by Navier-Stokes equations. Taking into account the

previously mentioned assumptions, the governing equations are:

$$\frac{\partial \rho}{\partial t} + \nabla \bullet (\rho U) = 0 \tag{2}$$

$$\rho \frac{DU}{Dt} = \rho \cdot g - \nabla P + \mu \nabla^2 U \tag{3}$$

where,

ρ: fluid density (kg/m^3)
U: velocity vector (m/s)
P: pressure (Pa)
g: gravity acceleration (m/s^2)
μ: fluid viscosity (Pa.s)

The outflow boundary conditions were assumed to be zero pressure at the flow outlet and no slip conditions at the vessel wall. The dynamic viscosity of blood and its density were assumed to be 3.5×10^{-3} Pa.s and 1050 kg/m^3, respectively[19-22]. The blood velocity boundary conditions were obtained from phase contrast MRI scanning. Figure 3 shows the mean velocity waveforms with a 0.8 sec period that were used as the inlet velocity conditions in the computational models[23]. The Reynolds number (*Re*) is the ratio of inertial to viscous forces and for a circular tube is given by:

$$\text{Re} = \frac{U_m D \rho}{\mu} \tag{4}$$

where,

D: characteristic length (diameter for artery)
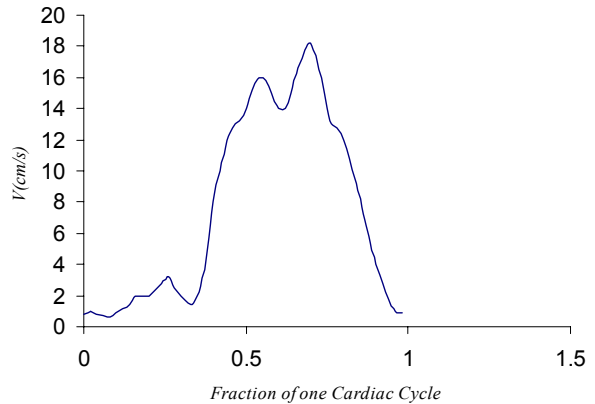U_m: average fluid velocity

Fig. 3: Flow waveform in the inlet of coronary artery models

In the case of pulsatile flow, the pulse rate was determined with the Womersley parameter, *α*, which

represents the ratio of unsteady to viscous forces and is defined as:

$$\alpha = \frac{D}{2}\sqrt{\frac{2\pi\rho f}{\mu}} \qquad (5)$$

where,

f: the frequency of the cardiac cycle (Hz)

Using the simulated flow conditions for a 2mm diameter tube, the calculated values for Womersley and Reynolds numbers were 1.53 and 100, respectively.

The commercial finite volume code FLUENT (version 6.0.12) was applied to solve the governing equations. FLUENT provides comprehensive modeling capabilities for a wide range of incompressible and compressible, laminar and turbulent fluid flow problems. In FLUENT, a broad range of mathematical models for transport phenomena (like heat transfer and chemical reactions) is combined with the ability to model complex geometries. FLUENT used a control-volume-based technique to convert the governing equations to algebraic equations that can be solved numerically. This control volume technique consists of integrating the governing equations about each control volume, yielding discrete equations that conserve each quantity on a control-volume basis.

Discretization of the governing equations can be illustrated most easily by considering the steady-state conservation equation for transport of a scalar quantity φ. This is demonstrated by the following equation written in integral form for an arbitrary control volume V as follows:

$$\oint \rho \varphi U \bullet dA = \oint \Gamma \varphi \nabla \varphi \bullet dA + \int_{V} S_{\varphi} dV \qquad (6)$$

where,

A: surface area vector

Γ_{φ}: diffusion coefficient for φ

S_{φ}: source of φ per unit volume

Equation 3 is applied to each control volume, or cell, in the computational domain. Discretization of Equation 1 on a given cell yields:

$$\sum_{f}^{N} U_{f} \varphi_{f} A_{f} = \sum_{f}^{N} \Gamma_{\varphi} (\nabla \varphi)_{n} A_{f} + S_{\varphi} V \qquad (7)$$

where,

N_{f}: number of faces enclosing cell

φ_{f}: value of φ convected through face f

U_{f}: mass flux through the face f

A_{f}: area of face f

V: cell volume

The equations solved by FLUENT take the same general form as the one given above and apply readily to multi-dimensional, unstructured meshes composed of arbitrary polyhedra. FLUENT stores discrete values of the scalar at the cell centers. However, face values φ_{f} are required for the convection terms in Equation 4 and must be interpolated from the cell center values. This is accomplished using an upwind scheme. In the upwind scheme, the face value φ_{f} is derived from quantities in the cell upstream, or upwind, relative to the direction of the normal velocity U_{n} in Equation 4. FLUENT allows us to choose from several upwind schemes: first-order upwind, second-order upwind, power law and QUICK.

Wall shear stress was determined as the product of viscosity and shear rate. Briefly, the fluent flow solver calculates shear rate (γ) and shear stress (τ) during incompressible and Newtonian fluids flow using Equation 5. The accuracy of the calculation was set at 10^{-4} m/sec, which resulted in an error of *WSS* of less than 1%.

$$\tau = \mu \cdot \gamma$$
$$\gamma = \frac{\partial U_{i}}{\partial x_{j}} + \frac{\partial U_{j}}{\partial x_{i}} \qquad (5)$$

The threshold for comparing distributions of low WSS between simulations was established at 0.5 Pa for comparison to previous work[24,25] and because vascular regions subjected to *WSS* below this value have been shown to strongly correlate with the sites of intimal thickening[4, 8, 26]. Regions of low *WSS* were also expressed as percentages of the stent area within intrastrut regions in the proximal, middle and distal portions of the stent in order to determine perturbations produced by stent strut geometry. Near-wall velocity vectors were also visualized at spatial locations in the proximal, middle and distal portions of the stent to observe the behavior of blood flow in these regions. The effect of the flow divider on these parameters was investigated, too.

RESULTS AND DISCUSSION

The results have shown that wall shear stress (*WSS*) distribution between stent struts was sensitive to stent strut spacing. This results show that depending on the ratio of strut width (*W*) to strut height (*H*) the flow separation zone and consequently, the *WSS* value changed markedly. Figure 4 illustrates the effects of stent strut spacing (*W/H*) on *WSS* during one cardiac cycle. To investigate the variation of *WSS* value with stent parameters, the mean of wall shear stress value in strut space without stent strut was considered and shown.

It can be seen that the *WSS* values in flow separation zones were considerably lower than those of the arterial without stent, which might contribute to
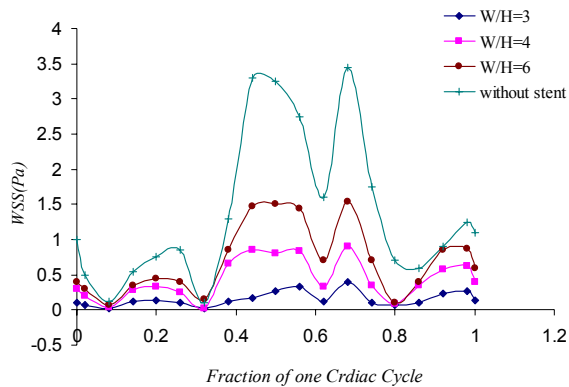
Fig. 4: Effect of the stent strut spacing *W/H* on the *WSS* value between stent struts
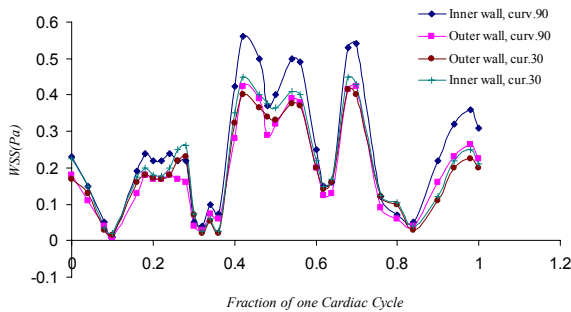

Fig. 5: Effect of curvature on the *WSS* value between stent struts for inner and outer wall

endothelial damage and consequently to the restenosis process. For stent strut spacing (*W/H* =3), flow separation zone covered all strut space and during 75% of cardiac cycle, the whole intrastrut area was exposed to distributions of *WSS* < 0.5 Pa. In this case, the mean *WSS* values during one cardiac cycle were less than 0.5 Pa. For stent strut spacing greater than 6 strut heights, the stagnation zones were separate and flow reattached to the wall between the wires. In this region, the maximum wall shear stress regained its value approximately to 80% of that of the arterial without stent. In the 70% of the cardiac cycle, mean *WSS* value in the stent strut spacing is greater than 0.5 Pa. When the stent strut space is *W/H*=4, in the 55% of the cardiac cycle, the mean *WSS* value in the stent strut spacing is greater than 0.5 Pa.

To investigate the effects of the arterial curvature and bending on *WSS* values, models of curved stented arteries with different curvature angles (30°, 60°, 90°) were analyzed. It is demonstrated that the *WSS* distribution is different along the inner and outer walls of the curved vessel. Models with different curvature

angles showed that the difference between inner and outer wall shear stress increases with increasing arterial curvature (Fig. 5).

The shear stress distribution within the flow divider increases with respect to the stent without flow divider. This increase within flow divider with different diameters is shown in Fig 6. When we used a flow divider with diameter (*D*/4), the *WSS* value along the wall between stent struts increased by a factor of 2. By increasing the diameter of the flow divider to *D*/3 and *D*/2, the flow pattern between stent struts was changed and the *WSS* value increased by a factor of 3 and 4, respectively.
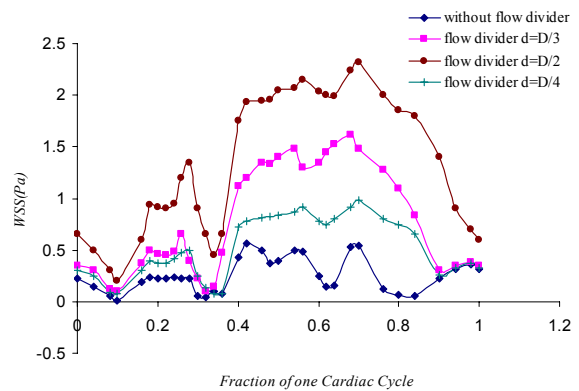

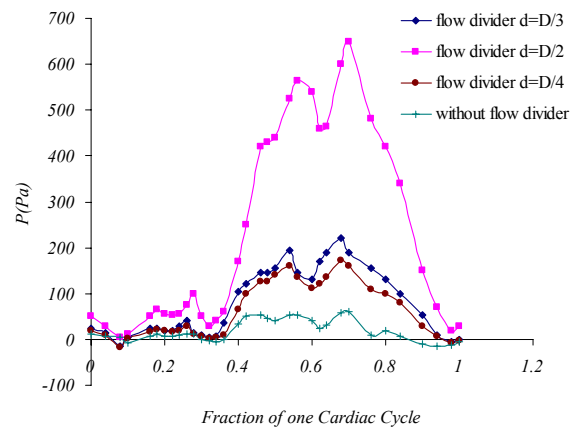Fig. 6: Effect of the flow divider on the *WSS* distribution between stent struts

Fig. 7: Additional pressure value across the stent including flow divider

The pressure gradient, according to stent and different diameter flow dividers, was calculated during the cardiac cycle. It is shown that the required pressure gradients in stented vessel cases are twice comparing the unstented vessel. Regarding the pressure gradient in

the flow divider with $D/4$ diameter, an increase of 4 times and for flow divider with $D/3$ and $D/2$ diameters an increase of 5 and 10 times is observed. Therefore, it is necessary to study the effect of this pressure on the vessels. In Fig. 7, the pressure values in the inlet of artery are shown on the vertical axis. The outflow boundary conditions were assumed to be zero pressure at the flow outlet. So, we can calculate the pressure gradient by dividing the pressure value to artery length.

Investigation of the wall shear stress distribution between stent struts, in pre-stent and post-stent regions in 3D model of stent with hexagonal strut shows that the presence of stents markedly affects the *WSS* distribution. The maximum *WSS* in the part of vessel, which is limited between the first stent strut, is the half of its value in unstented vessel and this amount will decrease during the stent length, too. This amount will decrease to 40% in the second loop comparing the unstented vessel. Values of *WSS* in the proximal of stent are more than the distal ones, so it is confirmed that the restenosis will increase in long stents (Fig. 8).
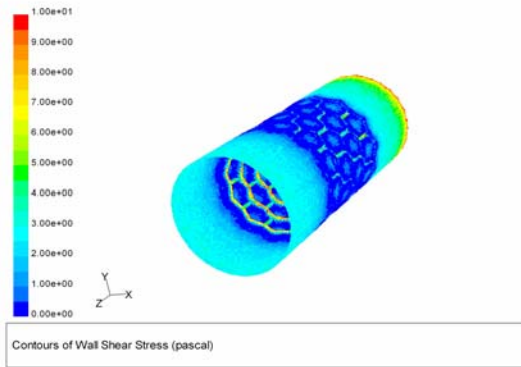

Fig. 8: Contours of *WSS* for stented coronary artery with hexagonal struts in the 0.4 Sec. from cardiac cycle
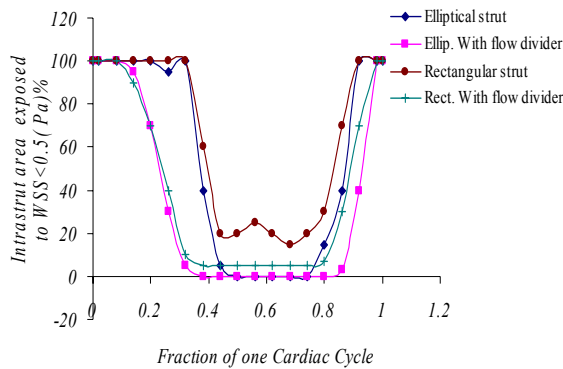

Fig. 9: Percentage of intrastrut area exposed to distributions of *WSS* < 0.5 Pa

This investigation for 3D models of stents with rectangular and elliptical stent struts was done as well and the first loop of a hexagonal, rectangular and elliptical stent struts are compared with each other (Fig. 9). The results show that the maximum values of *WSS* for rectangular, elliptical and hexagonal struts are equal, but the area is different. For a stent with rectangular strut, during 30% of cardiac cycle, the mean *WSS* value in the part of vessel (which is limited between the first stent strut) is greater than 0.5 Pa. For hexagonal and elliptical stent struts, this factor is 50%.

CONCLUSION

Some studies in the literature have suggested a link between stent design and restenosis. It is also clear that the local blood flow patterns are affected by stent design; hence, the relationships between blood flow patterns, stent design and the process of restenosis should be investigated thoroughly.

The current results confirm and extend our previous observations and further demonstrate the importance of stent geometry on intravascular fluid dynamics. The current findings with 3D computational fluid dynamics modeling demonstrate that with increasing the angle between two sides of the stent strut the percentage of intrastrut area that exposed to distributions of *WSS* < 0.5 Pa decreases. Therefore, the growth of intimal thickening in this area will decrease. So, the stent strut with elliptical geometry is more appropriate than those with hexagonal and rectangular geometry, respectively.

The results show that, the blood flow pattern in stented segment influenced by flow divider. The principle of the flow divider is based on the fact that for a given flow rate wall shear stress can be augmented significantly by placing a streamlined cylindrical body in the center of the arterial wall. The body deflects the central core of flow towards the wall, hence, increasing the wall shear stress between stent struts. There is a vortex in distal of the flow divider.

The size of this vortex changes during cardiac cycle. The flow separation zone decreases with increasing the size of this vortex. So, the *WSS* in this location increases markedly. The size of this vortex increased with increasing the flow divider diameter. By comparing the results for different diameters of flow divider, we can see that the optimum diameter for flow divider is $D/3$. Flow divider influences the blood flow pattern in proximal of stented segment, too. In this section, the *WSS* increases with application of the flow divider.

The current results further support the hypothesis that local flow patterns created by the stent should also be considered during stent design so as to minimize the indices of fluid dynamics implicated in neointimal hyperplasia.

ACKNOWLEDGEMENTS

REFERENCES

1. Lee, D. and J.J. Chiu, 1996. Intimal thickening under shear stress in a carotid bifurcation, a numerical study. J. Biomech., 29: 1-11.
2. LaDisa, J.F.J., L.E. Olson, R.C. Molthen, D.A. Hettrick, P.F. Pratt and M.D. Hardel, 2005. Alterations in wall shear stress predict sites of neointimal hyperplasia after stent implantation in rabbit iliac arteries. Am. J. Physiol. Heart Circ. Physiol., 288: 2465-75.
3. Najarian, S., J. Dargahi, F. Firouzi and F. Afsari, 2006. Unsteady simulation of distal blood flow in an end-to-side anastomosed coronary bypass graft with stenosis. Bio-Med. Mater. and Eng., 16: 337-347.
4. Mongrain, R. and J. Rodés-Cabau, 2006. Role of shear stress in atherosclerosis and restenosis after coronary stent implantation. Rev. Esp. Cardiol., 59: 1-4.
5. Farb, A, D.K. Weber and F.D. Kolodgie, 2002. Morphological Predictors of Restenosis after Coronary Stenting in Humans. Circulation, 105: 2974-2980.
6. Virmani, R., A. Farb, G. Guagliumi and F.D. Kolodgie, 2004. Drug-Eluting Stents: Caution and Concerns for Long-Term Outcome. Coronary Artery Disease, 15: 313-318.
7. Hayashi, K., Y. Yanai and T. Naiki, 1996. A 3D-LDV Study of the Relation Between Wall Shear Stress and Intimal Thickness in a Human Aortic Bifurication. ASME J. Biomech. Eng., 118: 273-279.
8. Danenberg, H.D., F.G. Welt and M. Walker, 2002. Systemic Inflammation Induced by Lipopolysaccharide Increases Neointimal Formation after Balloon and Stent Injury in Rabbits. Circulation, 105: 2917-2922.
9. Berry, J.L., J.E. Moore and W.D. Routh, 2000. Experimental and computational flow evaluation of coronary stents. Ann. Biomed. Eng., 28: 386-398.
10. Nicoud, F., H. Vernhet and M. Dauzat, 2005. A numerical assessment of wall shear stress changes after endovascular stenting. J. Biomech., 38: 2019-2027.
11. Kastrati, A., J. Mehilli and J. Dirsschinger, 2001. Restenosis after coronary placement of various stent types. Am. J. Cardiol., 877: 34-39.
12. LaDisa, J.F.J., L.E. Olson, R.C. Molthen, D.A. Hettrick, P.F. Pratt and M.D. Hardel, 2005. Circumferential vascular deformation after stent implantation alters wall shear stress evaluated using time-dependent 3d computational fluid dynamics models. J. Appl. Physiol., 98: 947-957.
13. LaDisa, J.F.J., L.E. Olson, R.C. Molthen, D.A. Hettrick, P.F. Pratt and M.D. Hardel, 2004. Stent design properties and deployment ratio influence indexes of wall shear stress: a three-dimensional computational fluid dynamics investigation within a normal artery. J. Appl. Physiol., 97: 424-430
14. Murata, T., T. Hiro and T. Fujii, 2002. Impact of the cross-sectional geometry of the post-deployment coronary stent on in-stent neointimal hyperplasia: an intravascular ultrasound study. Circulation, 66: 489-493.
15. Wentzel, J.J., R. Krams and J.C.H. Schuurbiers, 2001. Relationship between neointimal thickness and shear stress after wall stent implantation in human coronary arteries. Circulation, 103: 1740-1745.
16. Wentzel, J.J., D.N. Whelan, W.J. Vandergiessen and P.W. Serruys, 2000. Coronary Stent Implantation changes 3d vessel geometry and 3d shear stress distribution. J. Biomech., 33: 1287-1295.
17. Wentzel, J.J., F.J.H. Gijsen and N. Stergiopulos, 2003. Shear stress, vascular remodeling and neointimal formation. J. Biomech., 36: 681-688.
18. Carlier, S.G., J.J. Wentzel, P.W. Serruys and R. Krams, 2003. Augmentation of wall shear stress inhibits neointimal hyperplasia after stent implantation. Circulation, 107: 2741-2746.
19. Dehlaghi, V. and M. Tafazzoli-Shadpour, 2006. Analysis of pulsatile blood flow in stented human coronary arteries. Proce. of the 5th World Cong. of biomec., Munich, Germany.
20. Dehlaghi, V., M. Tafazzoli-Shadpour, S. Najarian and 2007. Analysis of 3D and steady blood flow in stented human coronary artery. Amirkabir J. Scie. Tech., Accepted for publication.

21. LaDisa, J.F.J., L.E. Olson, R.C. Molthen, D.A. Hettrick, D.C. Warltier, J.R. Kersten and P.S. Pagel, 2006. Alterations in regional vascular geometry produced by theoretical stent implantation influence distributions of wall shear stress: analysis of a curved coronary artery using 3D computational fluid dynamics modeling. J. Biomed. Eng. Online. 5: 40.

22. LaDisa, J.F.J., L.E. Olson, R.C. Molthen, D.A. Hettrick, D.C. Warltier, J.R. Kersten and P.S. Pagel 2005. Axial stent strut angle influences wall shear stress after stent implantation: Analysis Using 3D computational fluid dynamics models of stent foreshortening. J. Biomed. Eng. Online, 4: 59.

23. Suo, J., Y. Yang, J. Oshinski, A. Tannenbaum, J. Gruden and D. Gjddens, 2004. Flow patterns and wall shear stress distributions at atherosclerotic-prone sites in a human left coronary artery - an exploration using combined methods of CT and computational fluid dynamics. Proc. 26th Ann. Int. Conf. IEEE EMBS San Francisco, CA, USA. Sept. 1-5.

24. Kleinstreuer, C., S. Hyun, J.R. Buchanan, P.W. Longest, J.P. Archie and G.A. Truskey, 2001. Hemodynamic parameters and early intimal thickening in branching blood vessels. Crit Rev. Biomed. Eng., 29: 1-64.

25. DePaola, N., M.A.J. Gimbrone, P.F. Davies and C.F. Dewey, 1992. Vascular endothelium responds to fluid shear stress gradients. Arterioscler Thromb., 12: 1254-1257.

26. Garasic, J.M., E.R. Edelman, J.C. Squire, P. Seifert, M.S. Williams and C. Rogers, 2000. Stent and Artery Geometry Determine Intimal Thickening Independent of Arterial Injury. Circulation, 101: 812-818.